IOWA STATE UNIVERSITY
Digital Repository

Chemical and Biological Engineering Publications | Chemical and Biological Engineering

2000

Kinetic Model for Oxide Film Passivation in Aluminum Etch Tunnels

Nishant Sinha
Iowa State University

Kurt R. Hebert
Iowa State University, krhebert@iastate.edu

Follow this and additional works at: http://lib.dr.iastate.edu/cbe_pubs

Part of the Chemical Engineering Commons

The complete bibliographic information for this item can be found at http://lib.dr.iastate.edu/cbe_pubs/41. For information on how to cite this item, please visit http://lib.dr.iastate.edu/howtocite.html.

This Article is brought to you for free and open access by the Chemical and Biological Engineering at Iowa State University Digital Repository. It has been accepted for inclusion in Chemical and Biological Engineering Publications by an authorized administrator of Iowa State University Digital Repository. For more information, please contact digirep@iastate.edu.

Kinetic Model for Oxide Film Passivation in Aluminum Etch Tunnels

Abstract
Aluminum etch tunnels are micrometer-wide corrosion pits with large length-width aspect ratios, in which dissolution proceeds from the tip or end surfaces, while the sidewalls are covered by oxide films. The dynamics of oxide film passivation in etch tunnels has been investigated using decreasing current ramps superimposed on the otherwise constant applied current during anodic etching in 1 N HCl at 70°C. The ramps cause the dissolving area on the tip to be continuously reduced by passivation around its perimeter. Analysis of potential transients along with tunnel width profiles shows that two additive processes contribute to the passivation rate, expressed as the rate of decrease of actively dissolving area: a potential-dependent Tafel-type kinetic expression and a term proportional to the time derivative of the potential. The potential driving force is the "repassivation overpotential," the difference between the potential at the dissolving surface and the repassivation potential there. The kinetic model for passivation is consistent with both potential transients and tunnel width profiles, over a range of current ramp rates. The rate-controlling step of passivation is considered to be potential-dependent removal of chloride ions from the dissolving surface.

Disciplines
Chemical Engineering

Comments
This article is from *Journal of the Electrochemical Society* 147 (2000): 4111–4119, doi:10.1149/1.1394027.
Posted with permission.

This article is available at Iowa State University Digital Repository: http://lib.dr.iastate.edu/cbe_pubs/41

Journal of The Electrochemical Society, **147** (11) 4111-4119 (2000)
S0013-4651(00)02-013-9 CCC: $7.00 © The Electrochemical Society, Inc.

Kinetic Model for Oxide Film Passivation in Aluminum Etch Tunnels

Nishant Sinha[a] and Kurt R. Hebert*[,z]

Department of Chemical Engineering, Iowa State University, Ames, Iowa 50011, USA

Aluminum etch tunnels are micrometer-wide corrosion pits with large length-width aspect ratios, in which dissolution proceeds from the tip or end surfaces, while the sidewalls are covered by oxide films. The dynamics of oxide film passivation in etch tunnels has been investigated using decreasing current ramps superimposed on the otherwise constant applied current during anodic etching in 1 N HCl at 70°C. The ramps cause the dissolving area on the tip to be continuously reduced by passivation around its perimeter. Analysis of potential transients along with tunnel width profiles shows that two additive processes contribute to the passivation rate, expressed as the rate of decrease of actively dissolving area: a potential-dependent Tafel-type kinetic expression and a term proportional to the time derivative of the potential. The potential driving force is the "repassivation overpotential," the difference between the potential at the dissolving surface and the repassivation potential there. The kinetic model for passivation is consistent with both potential transients and tunnel width profiles, over a range of current ramp rates. The rate-controlling step of passivation is considered to be potential-dependent removal of chloride ions from the dissolving surface.
© 2000 The Electrochemical Society. S0013-4651(00)02-013-9. All rights reserved.

Manuscript submitted February 3, 2000; revised manuscript received July 10, 2000.

The stability of localized corrosion cavities such as pits is determined by whether the dissolving surface inside the cavity can be passivated by formation of an oxide film. The process of oxide film formation is therefore of fundamental importance to all types of localized corrosion phenomena. Many observations have been made about conditions which promote dissolution *vs.* passivation in pits.[1] Acidic pit solutions are necessary to prevent precipitation of oxide in the cavity solution.[2] High concentrations of aggressive anions such as chloride are also considered to be important to maintain dissolution.[1] Empirically, pits corrode freely only when the potential is more anodic than the critical repassivation potential, which is found to be a function of the aggressive anion concentration.[3-5]

These inferences about factors controlling oxide film formation have been taken from electrochemical measurements of the corrosion current on surfaces containing one or more pits. Direct observations of the microscopic details of oxide film formation are much more difficult, and few have been reported. For example, it is not known whether the film covers the dissolving surface as a front, or else forms as patches by two-dimensional nucleation, or by precipitation from the solution phase. These observations about the geometry of passivation would be relevant to the mechanism of the process, but are hindered by the typically high dissolution rate of the metal surface in the corrosion cavity, its small size, and the remoteness of its location. Interpretation of these observations would also be difficult, since the high dissolution rate also produces large concentration and potential gradients in the pit solution, such that identification of the local chemical driving force for passivation is a challenge.

Many of these typical problems with investigations of passivation can be avoided in studies of aluminum etch tunnels, making this phenomenon very attractive for fundamental characterizations of oxide film formation in corrosion pits. Tunnels are a geometrically unique variety of corrosion pit formed by anodic etching in chloride solutions at temperatures higher than about 60°C. Alwitt *et al.* describe phenomenological aspects of tunnel growth.[6] Tunnels widths are on the order of 1 μm, and they can grow to lengths of 100 μm. Dissolution proceeds from a tunnel's end, or tip surface, at equivalent current densities of 2-25 A/cm^2. Tunnels are oriented in the crystallographic <100> directions in the metal, and the dissolving tip surface is a smooth (100) plane. The flat dissolving surface at all tunnel lengths shows that the dissolution rate is uniform on the tip. There is no detectable dissolution on a tunnel's sidewalls during its growth, and since the tunnel width is either constant or a slowly decreasing function of depth, the passivity of the sidewalls extends to the end of the tunnel. Scanning electron microscopy (SEM) images show that the transition between tip and sidewall orientations occurs over a distance smaller than 100 nm. The large decrease of corrosion rate over this small distance is explained by the presence of a surface oxide film on the walls which does not cover the dissolving tip. Dissolution causes the tip to recede and new sidewall surface to be exposed, which evidently is rapidly passivated by oxide.

Passivation of the dissolving tip surfaces in tunnels can be induced in a controlled fashion by manipulation of the applied current during galvanostatic etching, and the progress of passivation then inferred from microscopic observations.[6-9] Tak *et al.* found that the initial effect of step reductions of applied current is to passivate portions of the interior of the tip surface, such that only small patches of dissolving area remain.[7,8] At later times, all but one of these patches passivate. Hebert and Alkire modulated the applied current by sawtooth waves rather than by steps.[9] They found that tunnel widths decrease continuously during the decreasing current ramp portion of these waveforms. Apparently, the ramps induce passivation only around the perimeter of the dissolving tip surface, rather than on its interior as in experiments with current steps.

Despite the highly concentrated solutions in tunnels, transport models can be readily constructed because the tunnel solution is approximately an $AlCl_3$ binary electrolyte, the tunnel geometry can be treated as one-dimensional, and transport is well approximated by steady-state diffusion and migration.[10-12] Tak showed that the driving force for passivation is a surface overpotential, in this paper denoted the "repassivation overpotential" η_R, defined as the difference between the potential at the dissolving surface and the empirical repassivation potential E_R.[7,8] E_R depends on the chloride concentration at the dissolving surface according to

$$E_R = E_R^0 - B \log C_t \qquad [1]$$

In the current step experiments, η_R falls quickly to a minimum in a time of about 0.1 ms after the step, and then relaxes in a few hundred milliseconds to its initial value. Tak showed that the fraction of the tip area passivated increases linearly as the minimum η_R becomes more negative, and that the period when patches passivate one-by-one is the same as the η_R relaxation time. Further, the time of less than 1 ms in which passivation occurs is much smaller than the time needed for the diffusion to change the solution composition at the tip. This suggests that η_R is the fundamental variable controlling passivation, as opposed to factors related to solution composition alone, such as chloride concentration or pH. Calculations of η_R during steady tunnel growth at constant applied current show that it remains smaller than 1 mV, for tunnel up to at least 15 μm in length.[12] Thus, the tips of all growing tunnels are poised at a potential close to E_R.

* Electrochemical Society Active Member.
[a] Present address: Micron Technology, Boise, ID.
[z] E-mail: krhebert@iastate.edu

Downloaded on 2014-02-10 to IP 129.186.176.91 address. Redistribution subject to ECS license or copyright; see ecsdl.org/site/terms_use

S0013-4651(00)02-013-9 CCC: $7.00 © The Electrochemical Society, Inc.

Tak and Hebert suggested that η_R controls the adsorption of chloride ions on the dissolving surface whose presence shields the surface from passivating water molecules.[8] Recently, evidence for adsorbate layers on various dissolving metal surfaces has been found by scanning tunneling microscopy (STM). Itaya and co-workers found ordered adsorbed layers of I on Pd, Ag, and Ni, as well as S on Ni, during dissolution processes.[13-16] Interestingly, the presence of the I layer on Pd and the S layer on Ni suppressed oxide passivation of these surfaces. Suggs and Bard, Vogt *et al.*, and Wan and Itaya all observed ordered chloride layers on Cu which remained on the surface during dissolution.[17-21] In all these examples, dissolution is found to proceed at surface steps.

In the present work, current ramps rather than current steps are used to initiate passivation. Ramps produce passivation around the perimeter of the dissolving tunnel tip, as opposed to the step experiments in which oxide forms in the interior of the tip.[9] Thus, ramps better simulate the type of passivation which occurs during the "natural" growth of tunnels at constant applied current, and the present kinetic measurements should be applicable to mathematical models of tunnel shape. The progress of passivation during current ramps is inferred by analysis of SEM images of tunnel shapes, and the repassivation overpotential driving force for passivation is determined from experimental potential transients. On the basis of these measurements, a kinetic model for passivation in etch tunnels is developed. The model seeks to reconcile the different morphology of oxide coverage in step *vs.* ramp experiments, and also attempts to further illuminate the physical and chemical processes which control passivation.

Experimental

The experimental materials, apparatus, and procedures were nearly the same as those described by Wiersma *et al.*[22] and Tak *et al.*[7] The aluminum foils used for etching were annealed, 99.98% pure, 100 μm thick, and their grain size is typically 100 μm (supplied by KDK Corp., Takahagi, Japan). Since tunnels penetrate the foil thickness without changing direction, it is apparent that the depth of grains is 100 μm. The foils were pretreated before etching by immersion in 1 N NaOH at room temperature for 10 min, which had been found to enhance uniformity of the distribution of tunnel lengths and widths. Etching was carried out using a controlled anodic current, in 1 N HCl solution at 70°C. The foil was placed in a glass holder exposing a circular area of 5 cm^2 on one side. The counter electrode was a Pt wire bent into a hoop and fixed in position on the exposed side of the holder. The reference electrode (Ag/AgCl/4 N KCl type, Fisher) was placed behind the holder and away from the current path between the working and counter electrodes. This electrode arrangement is meant to promote reproducibility of the cell ohmic resistance between experiments, and a uniform distribution of tunnels along the foil surface. Experiments consisted of applying a constant current of 40 mA/cm^2 for 5 s, and then initiating a decreasing current ramp. The ramp time and rate were experimental variables. Ramp rates of 10, 20, 40, 60, and 100 mA/cm^2-s were used. Etching current was supplied by a potentiostat/galvanostat (EG&G PAR 273) and the potential recorded using a voltmeter (Keithley 194A) interfaced to a personal computer. The morphology of tunnels was observed using the oxide replication technique developed by Dunn and Bolon.[23] The etched surface was anodized at 4 mA/cm^2 in 1.4 g/L ammonium phosphate solution to form a 70-75 V (80-90 nm thick) anodic oxide film, followed by dissolution of the aluminum metal in a solution of 10% Br_2 in methanol. The remaining oxide film was a replica of the tunnel morphology, and was sputter coated with gold for SEM observation. Further experimental details are provided by Sinha.[24]

Results and Discussion

Tunnel morphology during current ramps.—For the etchant bath composition and temperature used here, tunnels maintain a constant width for short etch times less than 10 s.[7] The current ramp causes the tunnel width to taper, as demonstrated by Fig. 1. The taper is due to the continuous encroachment of the dissolving tunnel tip surface by oxide film during the ramp time. The flat texture and orientation of the dissolving tip surface are unchanged by the ramp. This indicates that new oxide film does not form on the interior of the tip surface, but only along its edge. This mode of passivation, in which oxide coverage proceeds from the leading edge of the film on the tunnel sidewall, is similar to that during tunnel growth at constant current.

Figure 1. Example of an SEM of an oxide replica of an etch tunnel after experiments with a decreasing current ramp. Ramp rate 10 mA/cm^2-s, ramp time 2 s, 5 s at constant current (40 mA/cm^2) before ramp.

The metal dissolution rate during the ramp is found by measuring the effect of ramp time on the length of the tapered section. Figure 2 shows that the tunnel length increases at a constant rate during the ramp. The dissolution velocity obtained from the slope of Fig. 2 is 2.2 μm/s. The same velocity was found previously at these etching conditions by three measurements: extension of tunnel length at constant applied current[6]; wavelengths of tunnel width modulations induced by a periodically variable etching current[9]; and transient dissolution after step current reductions.[7] This mutual agreement

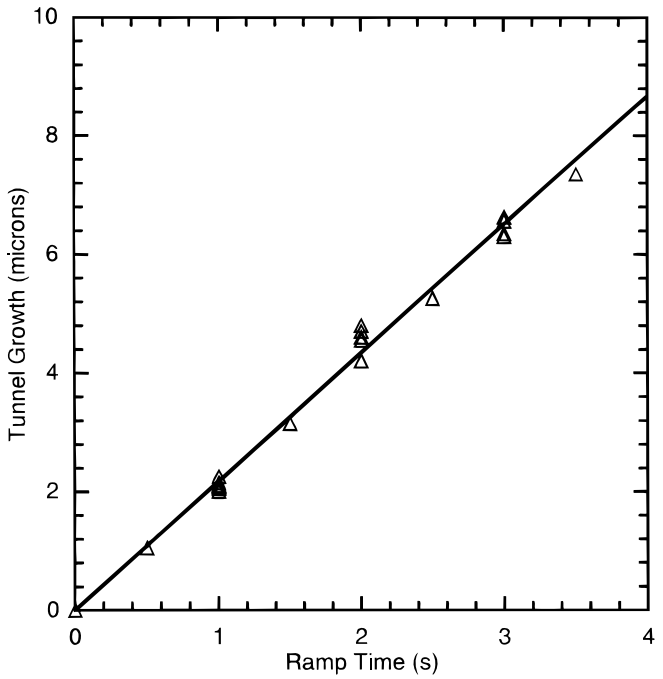

Figure 2. Increase of tunnel length during ramp as a function of ramp time. Current ramp rate is 10 mA/cm^2-s. Solid line is a regression fit to the data and has a slope of 2.17 μm/s.

Downloaded on 2014-02-10 to IP 129.186.176.91 address. Redistribution subject to ECS license or copyright; see ecsdl.org/site/terms_use

S0013-4651(00)02-013-9 CCC: $7.00 © The Electrochemical Society, Inc.

shows that the dissolution rate is unchanged by the application of current ramp or step reductions during etching.

During the ramps, the etching current can be adjusted not only by passivation, as suggested by Fig. 1, but also through variation of the rates of other processes such as cathodic hydrogen evolution, pit nucleation, and tunnel death. The significance of effects due to these other current sources is evaluated by comparing tunnel width profiles with current balance calculations, which assume that the fractional reduction of tip area at a given time is the same as the fractional reduction of applied current at that time. The current balance calculation of the width is

$$w(t) = w_0\left(\frac{i_a(t)}{i_{a0}}\right)^{1/2} \quad [2]$$

Figure 3 shows the width profiles of several tunnels from experiments with ramp rates of 10 and 20 mA/cm^2-s, where the dashed lines represent Eq. 2. While the data in Fig. 3 are limited, they demonstrate the following: (*i*) the passivation rate, as indicated by the width decrease during the ramp, is not the same in different tunnels on a surface, but appears to increase with tunnel width; (*ii*) the width decrease of small tunnels is larger than the current balance calculation, but that of wide tunnels approaches the calculation closely. This nonuniform behavior is understandable, since depending on the passivation mechanism, the width dependence of the passivation rate may not enable Eq. 2 to be enforced in individual tunnels. Thus, the current balance would be approached most closely by the widest tunnels, which dominate the overall electrode current due to the dependence of the tunnel current on the square of the width. Since Fig. 3 is consistent with this expectation, there is no evidence that processes other than passivation contribute significantly to the current decrease during the ramp.

Potential transients during current ramps.—Potential transients during the current ramps are shown in Fig. 4. All experimental potential transients shown in the paper are corrected for the cell ohmic resistance of 2.17 Ω-cm^2. [22] This value had been obtained from slopes of steady-state current-potential curves during etching, which were proportional to the etchant conductivity as well as consistent with the theoretically calculated cell ohmic resistance. The transients in Fig. 4a were measured in experiments where the current was reduced from 40 to 0 mA/cm^2. Generally, the potential at first decreases at an approximately constant rate, which becomes smaller after a time. When the current is small, the potential begins to decrease rapidly once again. The average slope of the potential transient is more negative for larger ramp rates.

The variability of transients for a given ramp rate is illustrated by Fig. 4b. The initial potential varies through a range of about 50 mV. The transients in Fig. 4b suggest that the overall slope of the transients at a given ramp rate is correlated with the initial potential: smaller

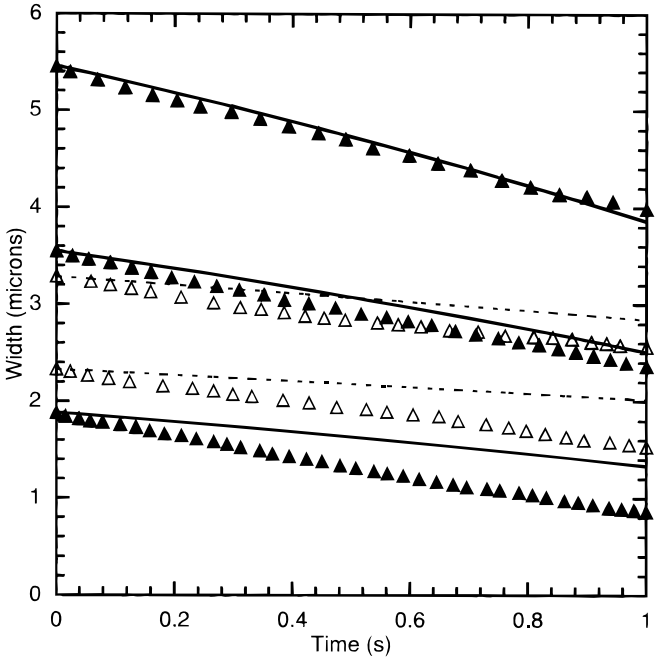

Figure 3. Comparison of measured tunnel widths during current ramps with current balance calculations. Symbols are width data and lines calculated values. Solid lines and solid symbols represent 20 mA/cm^2-s experiments and dashed lines and open symbols 10 mA/cm^2-s experiments.

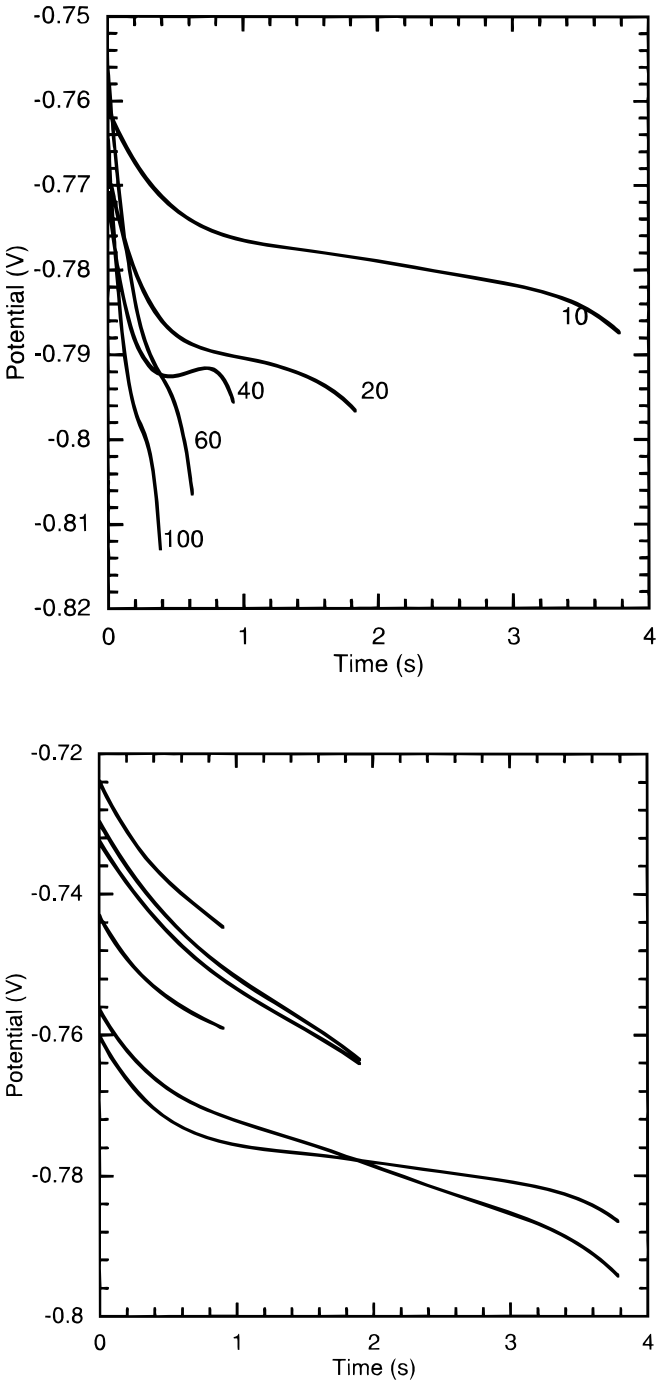

Figure 4. Potential transients during current ramps. (a, top) Effect of ramp rate on transients. Parameter is current ramp rate in mA/cm^2-s. (b, bottom) Several transients for a ramp rate of 20 mA/cm^2-s. Potentials are corrected using the measured value of the cell ohmic resistance.

Downloaded on 2014-02-10 to IP 129.186.176.91 address. Redistribution subject to ECS license or copyright; see ecsdl.org/site/terms_use

S0013-4651(00)02-013-9 CCC: $7.00 © The Electrochemical Society, Inc.

slopes are found in transients with more negative initial potentials. Sinha provides a fuller demonstration of this trend, using transients from a larger number of experiments.[24] One possible explanation for it is variability of the cell ohmic resistance between experiments. A larger-than-normal ohmic resistance would increase both the initial potential and the slope of the potential transient. The cell resistance measurements cited above indicate that the cell ohmic resistance varies about its mean value with a standard deviation of 0.38 Ω-cm^2 (18% of the mean resistance).[22] While an effort was made to maintain the same geometric arrangement of electrodes in the cell, small changes in electrode placement from one experiment to the next could account for both this scatter, and also the variability of the transients in Fig. 4b. For this reason, the variation of the cell resistance from the value of 2.17 Ω-cm^2 is included in the model as a parameter, denoted R'_Ω. The standard deviation of the fit values of this parameter is later compared with the expected value of 0.38 Ω-cm^2.

Interpretation of the potential measurements requires that they be related to the repassivation overpotential η_R, defined above as the potential measured with a reference electrode at the tip, relative to the repassivation potential for the solution present at the tip. Since the measurement of the potential uses a reference electrode in the bulk solution, it is necessary to determine the potential difference between reference electrodes in the bulk solution and at the tip. For calculation purposes, this potential difference is divided into several parts. One component is the potential drop between the bulk solution and the tunnel mouth, equivalent to the cell ohmic drop. Another is the "liquid junction potential" E_{LJ}, the potential drop between the tunnel mouth and tip. To simplify the calculation of E_{LJ}, a virtual Ag/AgCl reference electrode is assumed with the AgCl layer in direct contact with the local solution. The use of such a virtual electrode avoids the calculation of the potential drop across the glass membrane of the experimental Ag/AgCl/4 N KCl reference electrode. E_{LJ} may then be calculated using the method described by Newman[25]

$$E_{LJ} = \frac{1}{F}(\mu_-^b - \mu_-^t) = \int_0^L \frac{i_d}{\kappa} dz - \frac{4RT}{3F}\int_{C_b}^{C_t} t_+^0 d\ \ln(Cf_\pm) \quad [3]$$

The first term on the right side of the second equality represents the ohmic overpotential inside tunnels, and the second term is the concentration overpotential of the Ag/AgCl electrode. An additional potential drop must be added to the cell ohmic drop and E_{LJ}, namely, E_{RE}, the potential difference between the virtual Ag/AgCl reference electrode and the experimental Ag/AgCl/4 N KCl electrode, measured in the bulk solution. The relation between η_R and the potential E is then

$$\eta_R = E - i_a R'_\Omega - E_{RE} - E_{LJ} - E_R(C_t) \quad [4]$$

where $E_R(C_t)$ is the repassivation potential at the solution composition at the tunnel tip, as measured with an Ag/AgCl reference electrode. In Eq. 4, $i_a R'_\Omega$, E_{RE}, and $E_R(C_t)$ can in principle be obtained experimentally, while E_{LJ} can be calculated using a transport model. E is the potential corrected using the measured cell ohmic resistance, and R'_Ω represents the deviation of the true resistance from the measured value.

For convenience, the model equations developed below are given in terms of not η_R, but E_t, defined as the potential corrected for true cell ohmic drop, *i.e.*, $E_t = E - i_a R'_\Omega$. It can be demonstrated that η_R and E_t are equivalent to a good approximation. From Eq. 4

$$E_t = \eta_R + E_R(C_b) + E_{RE} + [E_{LJ} + E_R(C_t) - E_R(C_b)] \quad [5]$$

In the Appendix, the bracketed terms on the right side are calculated using a mass transport model. During current ramps as fast as 40 mA/cm^2-s, it is shown that the sum of these terms is no greater than 2 mV. Hence, the error due to the neglect of these terms is significantly smaller than the potential variations during the transients (Fig. 4). E_t is then equivalent to η_R augmented by the two additive constant terms $E_R(C_b)$ and E_{RE}, and may be used as a kinetic driving force for passivation.

Development of mathematical model for potential transients.—In Fig. 5, the potential transients from Fig. 4a are plotted as current-potential curves, which are directly compared with that from the step experiments.[8] The current is plotted on the abscissa as the fraction of the initial current. According to Fig. 3 and Eq. 2, this is approximately the same as the fraction of tip area not yet passivated. Thus, moving from right to left, the fractional tip area passivated increases from zero to one. The potential is shown as the potential decrease during the ramp. The line for the step experiments is supported by additional data not shown at smaller current fractions.

Figure 5 shows that, at early ramp times, all the ramp experiments, regardless of ramp rate, follow the same linear current-potential relationship as the step experiments. This initial period will be referred to as region 1. In region 1, the fraction of the initial tip surface area passivated is a linear function of the potential, and is independent of either the passivation rate, or whether the current reduction is in the form of a ramp or a step. Interestingly, however, during the ramps, passivation occurs only at the periphery of the dissolving surface, while in the step experiments portions of the interior of the tip are passivated. Thus, the morphology of passivation, but not the amount of area passivated, depends on the type of current reduction experiment.

The end of region 1 corresponds to a fractional current reduction of approximately 0.15. At this point, the slopes of the potential transients of ramp experiments decrease, and the current-potential curves diverge from the common line. The curves enter a region (region 2) where the lines for different ramp rates are separated. Generally, more negative potentials tend to be associated with faster ramps, but this trend is not rigorously followed. It is noted, though, that this trend can be partially "scrambled" by the expected variations of the cell ohmic resistance between experiments. The current-potential curves in region 2 are approximately linear up to fractional current reductions of about 0.8, at which point the potential begins to decrease sharply with current.

Important information about the passivation process during the ramp is conveyed by the behavior illustrated by Fig. 5. The straight

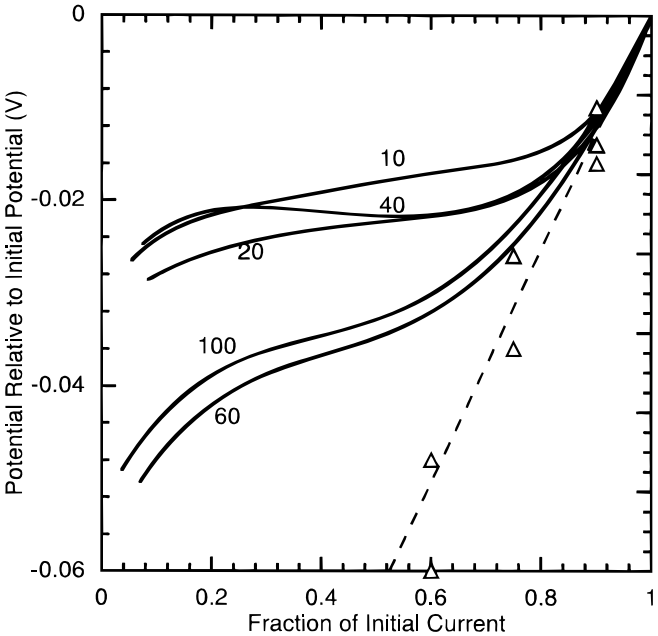

Figure 5. Plots of applied current density *vs.* potential for the ramp experiments in Fig. 4a, along with the plot of dissolution current density *vs.* potential from the current step reduction experiments of Tak and Hebert.[8] Parameter is current ramp rate in mA/cm^2-s. Solid lines and dashed line represent ramp and step experiments, respectively. Symbols represent some of the data from current step experiments, from which the dashed line was determined by regression. Potentials are corrected using the measured value of the cell ohmic resistance.

Downloaded on 2014-02-10 to IP 129.186.176.91 address. Redistribution subject to ECS license or copyright; see ecsdl.org/site/terms_use

S0013-4651(00)02-013-9 CCC: $7.00 © The Electrochemical Society, Inc.

line obeyed by the step experiments implies a linear relation between actively dissolving area and the potential driving force for passivation

$$\frac{dA(E_t)}{dE_t} = k_s A_0 \quad [6]$$

where the constant k_s has a value 7.94 V^{-1}.[8] Since this equation is also obeyed in region 1 of the current-potential curves for the ramp experiments, a relationship for dA/dt in region 1 may be obtained by differentiating Eq. 6 with respect to time

$$\frac{dA}{dt} = k_s w^2(t)\frac{dE_t}{dt} \quad [7]$$

Thus, at early times, while $w(t)$ is still approximately the same as the initial tunnel width w_0, the slope of the current-potential curve should be constant, as in Fig. 5.

According to Eq. 7, the rate of change of active area is proportional to the active area at a given time. This implies that the process which results in passivation can occur anywhere on the dissolving tip surface. On the other hand, the final outcome of passivation is the formation of oxide film on the outer edge of the tip. An explanation for this apparent paradox, as well as the different morphology observed in step and ramp experiments, might be given in terms of a chloride adlayer on the tunnel tip needed to maintain dissolution. In ramp experiments, chloride ions desorb from the interior of the dissolving surface, after which the resulting vacancies in the adsorbed layer diffuse to the edge of the tunnel tip. "Bare" metal surface unprotected by a chloride adlayer accumulates at the edge of the tip surface, where it is passivated by reaction with water. In the step experiments, a much higher concentration of vacancies would be formed in the interior of the adlayer, by the large number of nearly simultaneous desorption events at the time of the step. Owing to their high concentration, these vacancies would cluster together and form stable areas of bare surface on the interior of the tip, which are then passivated. The different morphology of passivation in the step and ramp experiments would result from the different time scales on which desorption occurs in these experiments.

In region 2 of Fig. 5, dA/dt, which is proportional to the ramp rate, depends on the potential. The dependence of the rate on potential indicates that, in this region, the decrease of active area is kinetically activated. It is assumed that reduction of the active area in region 2 results from a distinct chemical process from that which controlled in region 1, as would be the case if the region 1 and 2 processes occurred at different sites. While the region 1 process is considered to occur in the interior of the active tip, the region 2 process is taken to be localized at its perimeter. In the desorption model, such a process would be direct desorption of chloride ions from the edge of the dissolving surface. Desorption at the edge would be energetically distinct from desorption in the interior of the tip surface, because the chloride ions have different coordinative environments in the two kinds of sites; this energetic difference might account for different kinetic rate laws. dA/dt in region 2 is modeled as

$$\frac{dA}{dt} = -4w(t)k_p \exp\left(-\frac{\alpha F}{RT}(E_t - E_0)\right) \quad [8]$$

where the rate is represented by a Tafel expression and has units of rate of area change per unit length along the perimeter of the tip surface. With the Tafel form of the rate expression, the values of k_p, E_0, and α can be chosen such that the contribution of Eq. 8 is not significant in region 1, but dominates over that from Eq. 7 in region 2.

While the tunnel tip surface recedes as a result of dissolution, new sidewall surface is continuously exposed. The passivity of the tunnel sidewalls shows that this new surface must be rapidly covered with oxide. At this point, it is necessary to decide whether the initial state of this new surface is "active" in the sense that it is covered with a chloride surface layer inhibiting passivation. If the new sidewall surface is initially active, then it should be included in dA/dt in Eq. 7 and 8; chloride ions would need to be continuously removed from the new area to permit its passivation. On the other hand, continuous "deactivation" of the new sidewall area would not be necessary if it had never been covered with a chloride layer, since the surface would passivate spontaneously upon its exposure. While the atomic scale dissolution mechanism is not known, the crystallographic texture of the dissolving surface may suggest a layer-by-layer process, in which dissolution is localized on steps separating atomically flat (100) terraces.[13-21] The new sidewall surface would then correspond to the edges of these steps, and as the steps migrate toward the tunnel sidewalls, the new surface would accumulate there. In terms this atomic-scale model, the two limiting cases under consideration would be that chloride ions either adsorb on the step edges before the steps migrate to the sidewalls, or else the step edges are free of chloride.

Because of this uncertainty, it is not clear whether rate of change of "active" area in Eq. 7 and 8 should include sidewall area newly generated by dissolution. Hence, two alternative expressions for dA/dt are considered, and then developed as models for potential transients. If the new sidewall area is not covered by adsorbed chloride, the expression

$$\frac{dA}{dt} = 2w\frac{dw}{dt} \quad [9]$$

is used. Note that in this case the rate of change of active area in Eq. 9 is not equivalent to the rate of area passivated. The passivated area additionally includes a new sidewall area which had never been active since it was not covered with a chloride layer. The alternative to Eq. 9 is that the new surface is active; in this case, the rate of area passivated and the rate of decrease of active area are the same. The differential area passivated can then be expressed in terms of the differential change in length of the oxide-covered sidewall surface

$$\left(\frac{dA}{4w}\right)^2 = (v_d dt)^2 + \left(\frac{dw}{2}\right)^2 \quad [10]$$

where dA is the differential decrease of active area or increase of passive area, dw is the accompanying decrease of tunnel width, and v_d is the metal dissolution rate. The term on the left side is the differential length passivated, which is resolved on the right side into components along the directions parallel and perpendicular to the tunnel axis. An expression for dA/dt is obtained by differentiating Eq. 10 with respect to time

$$\frac{dA}{dt} = -4w\left[v_d^2 + \frac{1}{4}\left(\frac{dw}{dt}\right)^2\right]^{1/2} \quad [11]$$

The validity of either Eq. 9 or 11 is to be judged on the basis of how well the model resulting from either equation is able to predict the observed potential transients.

The models for the potential transients are formulated from current balance equations which assume that the contributions from Eq. 7 and 8 are additive. The need for both processes is demonstrated by noting that if Eq. 8 alone controlled passivation, there would be a discontinuous jump of the potential when the current ramp is initiated; hence, Eq. 7 is also needed to explain the continuity of the transients at this time. Accordingly, Eq. 7 and 8 are added together, and the result substituted into either Eq. 9 or 11. The tunnel width w is set by the current balance (Eq. 2). The model based on Eq. 9 is denoted model A, and that resulting from Eq. 11 is called model B. The differential equation describing model A is

$$\frac{dE}{dt} = \frac{4k_p}{k_s w}\exp\left\{-\frac{\alpha F}{RT}[E - E_0 - i_{a0}R'_\Omega(1 - v_R t)]\right\} - i_{a0}v_R R'_\Omega - \frac{4}{k_s w}\left(v_d^2 + \frac{w_0^4 v_R^2}{16w^2}\right)^{1/2} \quad [12]$$

The equation for model B is

Downloaded on 2014-02-10 to IP 129.186.176.91 address. Redistribution subject to ECS license or copyright; see ecsdl.org/site/terms_use

S0013-4651(00)02-013-9 CCC: $7.00 © The Electrochemical Society, Inc.

$$\frac{dE}{dt} = \frac{4k_p}{k_s w}\exp\left\{-\frac{\alpha F}{RT}[E - E_0 - i_{a0}R'_\Omega(1 - v_R t)]\right\} - i_{ao}v_R R'_\Omega - \frac{v_R w_0^2}{k_s w^2} \quad [13]$$

where v_R is the current ramp rate divided by the initial current. As mentioned earlier, the potential E in Eq. 12 and 13 is the potential after correction for the measured ohmic resistance. E and E_t are related by

$$E_t = E - i_{a0}(1 - v_R t)R'_\Omega \quad [14]$$

The terms $i_{a0}v_R R'_\Omega$ in Eq. 12 and 13 come from differentiation of this equation according to Eq. 7. The potential parameter E_0 was arbitrarily chosen to be −0.700 V *vs*. Ag/AgCl/4 N KCl, and w_0 was set to 4.0 μm, representative of the larger tunnel widths.

Comparison of model predictions with experimental potential transients and tunnel width profiles.—The three unknown model parameters are R'_Ω and the kinetic parameters k_p and α. For the potential transients in Fig. 4a, R'_Ω was determined for each transient from the corresponding current-potential curves in Fig. 5, by measuring the slope of the extended linear portion of the curves in region 2. Since region 2 was most pronounced in the 10 and 20 mA/cm^2-s transients, k_p and α were determined from these transients with the help of a nonlinear optimization algorithm which minimized the integrated square deviation between the model and the potential transients.[24] R'_Ω could not be calculated directly from the transients in Fig. 4b because the region 2 portions of these transients are not sufficiently developed. Thus, once k_p and α had been determined from the transients in Fig. 4a, those in Fig. 4b were fit to the model by allowing the optimization algorithm to adjust R'_Ω for each transient. The model differential equations were integrated numerically using a Gear algorithm.

Model A is found to yield a poor representation of the experimental transients, especially in the linear portion at small times (region 1). The failure of this model in region 1 is illustrated by the predicted current-potential curves, shown in Fig. 6. These curves at the different ramp rates are separated in region 1, and not collinear as are the experimental curves in Fig. 5. The reason for this behavior can be appreciated by examining Eq. 12. The dominant terms in region 1 are the last two terms on the right side of this equation. When only these terms, along with the time derivative, are included in the equation, Eq. 12 should reduce to Eq. 7, which is the equation expressing the common behavior of the transients in region 1. However, the two equations are not equivalent under these conditions because of the presence of the v_d^2 factor in the last term of Eq. 12. Since this factor represents chloride removal from newly generated sidewall area, it is concluded that the new area must not be covered by a chloride layer.

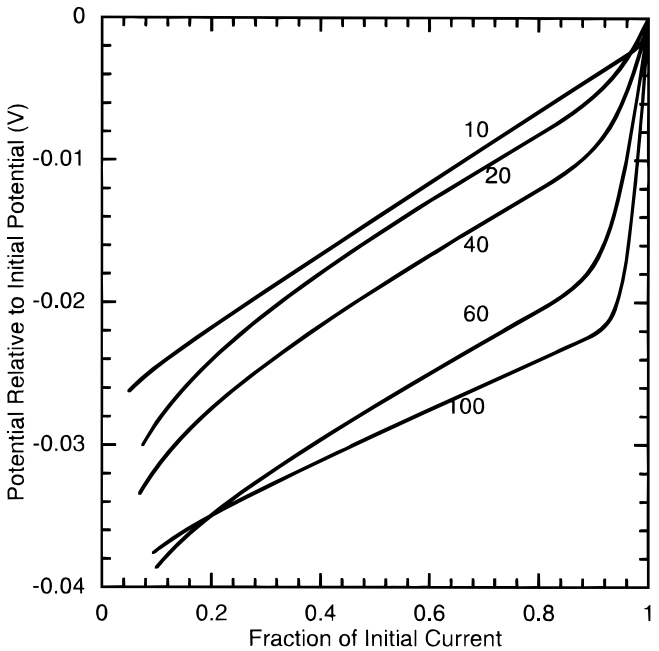

Figure 6. Current-potential curves predicted by model A after fitting kinetic parameters and cell resistance to experimental potential transients in Fig. 4a. Potentials are corrected using the measured value of the cell ohmic resistance.

In contrast to model A, model B reduces to Eq. 7 at small times, and therefore displays the experimentally observed common behavior in region 1 for different ramp rates. Figure 7a shows a set of potential transients at different ramp rates predicted by model B, after fitting the kinetic parameters and the cell resistance. In Fig. 7b, several potential transients for a ramp rate of 10 mA/cm^2-s are given. Both figures also display the experimental transients from Fig. 4 for comparison. The values of k_p and α obtained by fitting are 6×10^{-7} μm/s and 4.5, respectively. It is seen that exact agreement with the experimental transients at early times is always obtained, which demonstrates that the predicted current-potential plots, like the experimental ones, are collinear in region 1. The model yields good quantitative agreement with all the experimental transients shown. Aside from the region 1 behavior, the model potential transients produce other important features of the experimental transients: points of inflection, extended linear portions in region 2, and accelerating potential decays as the current approaches zero. The linearity in region 2, and the similar slopes of the current-potential plots (Fig. 5) in this region, are attributed to the influence of the cell ohmic resistance. The rates of potential decay increase at long times because both the area and the perimeter of the dissolving tip are reduced significantly; according to Eq. 7 and 8, the potential must decrease more rapidly in order to maintain the same rate of decrease of active area.

The superior effectiveness of model B relative to A is fundamentally significant for the passivation mechanism. The distinction between the models lies in the meaning of the area dA/dt in Eq. 9 and 11. In Eq. 9 (model B), dA/dt represents the rate of change of continuously dissolving area on the tunnel tip. Model A and Eq. 11, however, view dA/dt essentially as the rate of change of passivated area. The failure of model A shows that the passivation model cannot be expressed in terms of the rate of oxide coverage, even though it may be intuitively appealing to do so. Instead, it should be written in terms of the rate of removal of the chloride layer from the active surface. This latter process must then be the rate-determining step in passivation.

As discussed above, the cell resistance was adjusted individually in fitting the various potential transients. When instead a single-cell resistance is used for all the transients, generally poor agreement with the experimental measurements is obtained.[24] The standard deviation of the fit cell resistances is 0.36 Ω-cm^2, which agrees very closely with the standard deviation of the measured cell resistance, 0.38 Ω-cm^2. [22] Hence, the presently observed variability of R'_Ω is exactly as should be expected, if R_Ω in fact represents the cell resistance. The differences between the transients in Fig. 4b and 7b are therefore due to small variations of R_Ω between experiments. After ohmic correction using R'_Ω, the standard deviation of the initial potential variation is only 6.4 mV, compared to 18 mV without this correction. The small variation of the initial potential between experiments ($E_t = -0.773$ V ± 3 mV [95% confidence interval]) suggests that stable tunnel growth is associated with a very narrow range of potentials.

As described above, desorption in region 2 is considered to occur directly from the perimeter of the adsorbed layer. An alternative model in which it takes place from sites within the adlayer, followed by vacancy diffusion to the perimeter, is described by Sinha.[24] The quality of the fit by this model to the experimental potential transients is quite good, similar to that obtained with model B. However, model B is favored since as discussed above it is considered that desorption in regions 1 and 2 should occur from distinct sites.

Downloaded on 2014-02-10 to IP 129.186.176.91 address. Redistribution subject to ECS license or copyright; see ecsdl.org/site/terms_use

S0013-4651(00)02-013-9 CCC: $7.00 © The Electrochemical Society, Inc.

After the kinetic parameters had been established by fitting, the model was used to predict the decrease of the tunnel width with time during the current ramp. Equation 13 is used for this purpose, but $w(t)$ is treated as an unknown variable rather than assuming that it follows the current balance (Eq. 2). The potential transient in the experiment for which w is to be predicted was fit to a fifth-order polynomial, which is used to evaluate E and dE/dt in Eq. 13. The model equation then becomes a first-order linear differential equation in $w(t)$

$$\frac{dw}{dt} = -2k_p \exp\left[-\frac{\alpha F}{RT}(E_t - E_0)\right] + \frac{1}{2}k_s \frac{dE_t}{dt} w \qquad [15]$$

where Eq. 14 is used to determine E_t. This equation was integrated numerically. The initial condition for w is the tunnel width at the time when the ramp was initiated, and was taken from measurements of individual tunnels from Fig. 3. Predicted width profiles are shown in Fig. 8, along with the experimentally measured profiles and those calculated by enforcing the current balance (Eq. 2) in each tunnel. Overall, the agreement with the width measurements is good, but not appreciably different from their agreement with the current balance calculation. Nevertheless, this calculation is important to show consistency between the width measurements and the model.

The modeling results may be used to explain the observation that the widths of short tunnels do not change during their growth at constant applied current. As mentioned earlier, steady tunnel growth at constant current is associated with an E_t value close to −0.773 V. At this potential, the contribution of the Tafel term in Eq. 15 to the rate of decrease of tunnel width is 0.078 μm/s, much smaller than the dissolution velocity of 2.1 μm/s. Since E_t and η_R are directly related by Eq. 5, the previous calculation of η_R shows that E_t decreases by less than 1 mV during growth of a tunnel up to a length of 15 μm.[12] An even larger 5 mV decrease of E_t would increase the Tafel term to only 0.17 μm/s. Because the predicted η_R changes slowly with tunnel length, the time derivative term in Eq. 15 would be even less significant than the Tafel term. Therefore, it is clear that there should be no significant change of the size of the active tip surface during the growth of short tunnels. Apparently, the driving force for chloride desorption from the tip during tunnel growth is very small. The constant tunnel width is then expected from the kinetic model.

Conclusions

The present work, coupled with that of Tak *et al.*[7,8] has provided a detailed picture of the dynamics of passivation in aluminum etch tunnels. In both current step and current ramp experiments, tunnel morphology studies have allowed the time-dependent geometry of oxide film coverage to be inferred. In this work, mathematical descriptions of passivation have been formulated from analysis of potential transients and tunnel width profiles during ramp experiments. The models are based on knowledge of the concentration and potential at the dissolving surface during passivation, which was

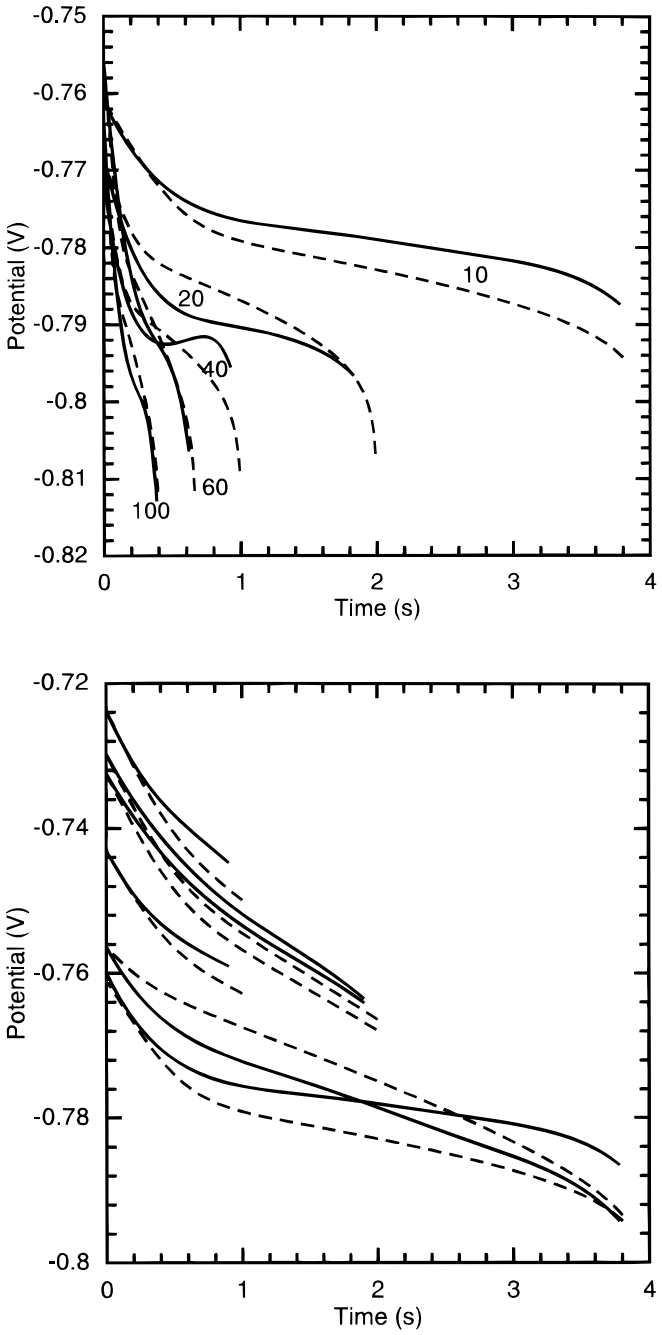

Figure 7. Comparison of experimental potential transients (solid lines) with those predicted by model B (dashed lines). (a, top) Potential transients for various current ramp rates. (b, bottom) Several transients at a ramp rate of 10 mA/cm^2-s. Potentials are corrected using the measured value of the cell ohmic resistance.

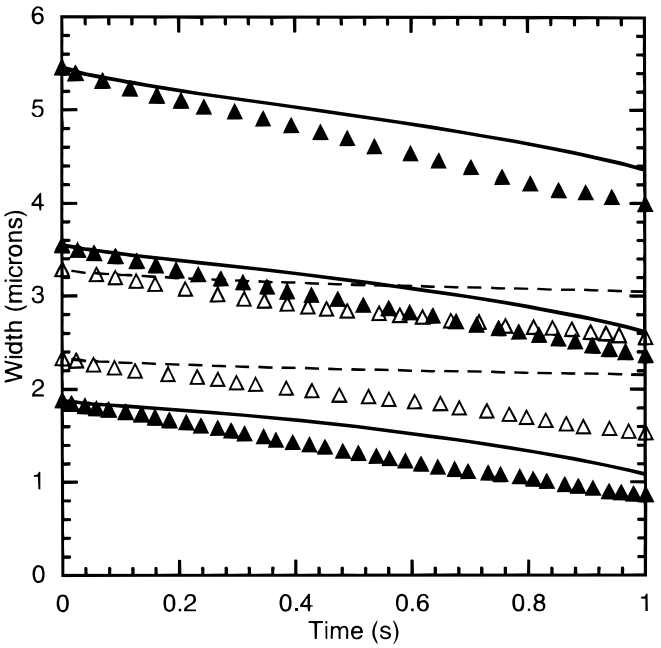

Figure 8. Comparison of measured tunnel widths during ramps with predictions by model B. Symbols are width data and lines model calculations. Solid lines and solid symbols represent 20 mA/cm^2-s experiments and dashed lines and open symbols 10 mA/cm^2-s experiments.

Downloaded on 2014-02-10 to IP 129.186.176.91 address. Redistribution subject to ECS license or copyright; see ecsdl.org/site/terms_use

S0013-4651(00)02-013-9 CCC: $7.00 © The Electrochemical Society, Inc.

determined with the help of transport models. The rate of decrease of the active area is found to be composed of two additive contributions, one term proportional to the time derivative of the potential and the other term a Tafel-type rate expression in terms of the potential itself. Thus, the importance of the potential as the controlling variable for passivation is reinforced. Specifically, the potential driving force is the "repassivation overpotential," which is the difference between the local potential at the dissolving surface and the value of the repassivation potential there. While it is premature to generalize this finding, a critical repassivation potential is found in many different metal-electrolyte systems exhibiting localized corrosion, and the present model offers a simple explanation for its significance. It is also consistent with other empirical ideas that pit stability is favored by factors such as high potentials and high chloride ion concentrations in the pit.[1] Critical acidification as a criterion for pit stability is not supported by the present results, although it may apply to pitting in solutions of higher pH for which oxide precipitation is possible.[2] It is found here that passivation can be modeled most effectively in physical terms by desorption of chloride ions from an adsorbed layer on the dissolving surface. The presence of such a layer during dissolution is consistent with recent STM studies of other systems.[13-21]

Acknowledgments

Support for this work was provided by KDK Corporation and by St. Jude Medical. Aluminum foils were provided by KDK Corporation.

Appendix

This Appendix describes the calculation of the potential correction $E_{LJ} + E_R(C_t) - E_R(C_b)$ in Eq. 5. This correction is given by

$$E_{LJ} + E_R(C_t) - E_R(C_b) = \int_0^{v_d t} \frac{i_d}{\kappa} dz - \frac{4RT}{3F} \int_{C_b}^{C_t} t_+^0 d \ln(Cf_\pm) - 0.0337 \log \frac{C_t}{C_b} \quad [A\text{-}1]$$

where the first two terms on the right side represent E_{LJ}, and the 0.0337 factor is the empirical parameter B in Eq. 1.[12] The conductivity, transference number, and activity coefficient are experimentally derived functions of concentration. Hence, the concentration profile in the tunnel must first be found in order to calculate the potential correction. Equation A-1 models the tunnel in terms of a one-dimensional rectangular coordinate system with position coordinate z.

The concentration profile is obtained by solving the diffusion equation in the tunnel, given previously for this coordinate system as[12]

$$\tau^2 \frac{\partial \theta}{\partial \tau} = -(1 - x)\frac{\partial \theta}{\partial x} + N\frac{\partial^2 \theta}{\partial x^2} \quad [A\text{-}2]$$

where x is the reduced position coordinate in tunnels, $x = z/(v_d t)$. $z = x = 0$ refers to the tunnel mouth and $z = v_d t$ and $x = 1$ to the tunnel tip. θ and τ represent dimensionless concentration and time, respectively. Their definitions are $\theta = C/C_b$, and $\tau = (i_d t_-^0 v_d t)/(3FDC_b)$. N is a dimensionless parameter, $N = (\rho t_-^0)/(C_b M)$, which is related to the ratio of the aluminum concentration in the metal to that in the solution. Equation A-2 models the tunnel solution as an $AlCl_3$ binary electrolyte, which is valid because hydrogen ions are driven out of the tunnel by migration.[12] The term on the left side of Eq. A-2 accounts for transient changes in concentration in the tunnel, and the first term on the right side represents convection effects, due to both the moving boundary at the tunnel tip and to the flow of liquid into the volume vacated by metal dissolution. The second term on the right side of Eq. A-2 is due to the diffusion of the binary electrolyte. When N is large and τ is small, the concentration profile is nearly the same as the steady-state profile at a given tunnel length. The boundary conditions for Eq. A-2 are

$$\theta(x = 0) = 1$$

$$\frac{\partial \theta}{\partial x}(x = 1,\ t < 5\text{s}) = \tau \quad [A\text{-}3]$$

$$\frac{\partial \theta}{\partial x}(x = 1,\ t \geq 5\text{s}) = \tau[1 - v_R(t - 5\text{s})]$$

According to the first condition, the bulk solution is taken to be an $AlCl_3$ solution with the same chloride ion concentration as that of the HCl etchant, but with Al^{+3} ions substituted for H^+ ions. The second condition expresses the continuity of the rates of production of Al^{+3} ions by dissolution and their transport into the solution. It is assumed that the ramp is initiated after a 5 s period at constant applied current.

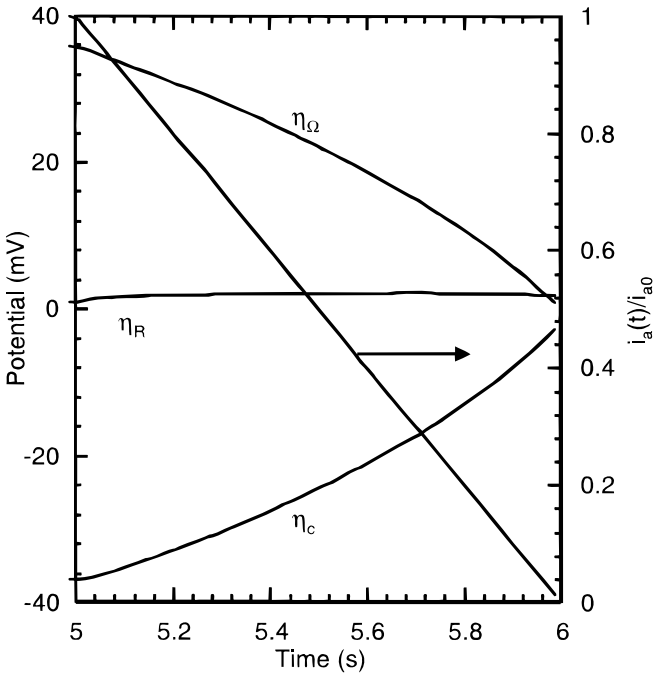

Figure A-1. Ohmic and concentration overpotentials in tunnel during current ramp. Ramp rate of 40 mA/cm^2-s applied after 5 s of etching at constant applied current.

Equation A-2 and A-3 were solved numerically using the D03PHF subroutine of the NAG library (method of lines using spatial discretization with finite differences). In the calculation, the etching temperature is 70°C, and the chloride concentration in the etchant bath is 1 N. The value of N is 240. The fractional current ramp rate is $v_R = 1.0\ s^{-1}$, corresponding to a current ramp of 40 mA/cm^2-s. Figure A-1 shows the components of the potential correction as a function of time during the ramp: ohmic overpotential (first term in the right side of Eq. A-1) and concentration overpotential (sum of remaining two terms). While the magnitudes of these overpotentials are as large as 40 mV, their sum is no greater than 2 mV during the ramp. This potential correction is smaller than 1 mV if pseudo-steady state diffusion in the tunnel is assumed.[12] Thus, in the ramp experiments, nearly pseudo-steady diffusion is maintained even in the presence of transient effects due to the current ramp and tunnel growth. The potential correction in Eq. A-1 can be assumed to be zero with the introduction of only a small error of 1 or 2 mV.

List of Symbols

A	active tunnel tip area, cm^2
A_0	active tunnel tip area at start of current ramp, cm^2
C	binary electrolyte concentration, mol/cm^3
C_t	binary electrolyte concentration at tunnel tip, mol/cm^3
C_b	binary electrolyte concentration in bulk solution, mol/cm^3
D	binary electrolyte diffusion coefficient, cm^2/s
E	measured potential corrected with cell ohmic resistance of 2.17 Ω-cm^2, V
E_R	repassivation potential of aluminum, V
E_t	measured potential corrected for true cell ohmic resistance, V
E_0	potential parameter in passivation rate expression, V
F	Faraday's constant, 96,487 C/equiv
$f_\pm$	mean molar activity coefficient of an electrolyte
i_a	applied current density, A/cm^2
i_{a0}	applied current density at start of current ramp, A/cm^2
i_d	tunnel dissolution current density ($3Fv_d\rho/M$), A/cm^2
k_p	passivation rate constant, cm/s
k_s	passivation rate constant, V^{-1}
L	tunnel length, cm
M	atomic mass of aluminum, g/mol
N	dimensionless parameter in binary electrolyte diffusion equation
R	gas constant, 8.314 J/mol-K

Downloaded on 2014-02-10 to IP 129.186.176.91 address. Redistribution subject to ECS license or copyright; see ecsdl.org/site/terms_use

S0013-4651(00)02-013-9 CCC: $7.00 © The Electrochemical Society, Inc.

R_Ω cell ohmic resistance, Ω-cm^2
R'_Ω difference between cell ohmic resistance and reference value of 2.17 Ω-cm^2
T absolute temperature, K
t time, s
t^0_+, t^0_- cation and anion transference numbers of binary electrolyte
v_d metal dissolution velocity in tunnel, cm/s
v_R current ramp rate divided by initial current, s^{-1}
w width of tunnel tip surface, cm
w_0 width of tunnel tip surface at start of current ramp, cm
x reduced position coordinate along tunnel axis, dimensionless
z position coordinate along tunnel axis, cm

Greek

α transfer coefficient, dimensionless
η_R repassivation overpotential, V
κ solution conductivity, (Ω-cm)$^{-1}$
μ^t_-, μ^b_- electrochemical potentials of chloride ions at the tunnel tip and in bulk solution, J/mol
θ binary electrolyte concentration, dimensionless
ρ density of metal, g/cm^3
τ time, dimensionless

References

1. G. S. Frankel, *J. Electrochem. Soc.*, **145**, 2186 (1998).
2. J. R. Galvele, *J. Electrochem. Soc.*, **123**, 464 (1976).
3. J. R. Galvele, in *Passivity of Metals*, R. P. Frankenthal and J. Kruger, Editors, p. 285, The Electrochemical Society Corrosion Monograph Series, Princeton, NJ (1978).
4. H. Kaesche, in *Passivity of Metals*, R. P. Frankenthal and J. Kruger, Editors, p. 935, The Electrochemical Society Corrosion Monograph Series, Princeton, NJ (1978).
5. N. G. Thompson and B. C. Syrett, *Corrosion*, **48**, 649 (1992).
6. R. S. Alwitt, H. Uchi, T. R. Beck, and R. C. Alkire, *J. Electrochem. Soc.*, **131**, 13 (1984).
7. Y. Tak, E. R. Henderson, and K. R. Hebert, *J. Electrochem. Soc.*, **141**, 1446 (1994).
8. Y. Tak and K. R. Hebert, *J. Electrochem. Soc.*, **141**, 1453 (1994).
9. K. Hebert and R. Alkire, *J. Electrochem. Soc.*, **135**, 2447 (1988).
10. K. Hebert and R. Alkire, *J. Electrochem. Soc.*, **135**, 2146 (1988).
11. D. Goad, *J. Electrochem. Soc.*, **144**, 1965 (1997).
12. Y. Zhou and K. R. Hebert, *J. Electrochem. Soc.*, **145**, 3100 (1998).
13. K. Sashikata, Y. Matsui, K. Itaya, and M. P. Soriaga, *J. Phys. Chem.*, **100**, 20027 (1996).
14. T. Teshima, K. Ogaki, and K. Itaya, *J. Phys. Chem. B.*, **101**, 2046 (1997).
15. P. Muller, S. Ando, T. Yamada, and K. Itaya, *J. Electroanal. Chem.*, **467**, 282 (1999).
16. S. Ando, T. Suzuki, and K. Itaya, *J. Electroanal. Chem.*, **412**, 139 (1996).
17. D. W. Suggs and A. J. Bard, *J. Am. Chem. Soc.*, **116**, 10725 (1994).
18. D. W. Suggs and A. J. Bard, *J. Phys. Chem.*, **99**, 8349 (1995).
19. M R. Vogt, F. A. Möller, C. M. Schilz, O. M. Magnussen, and R. J. Behm, *Surf. Sci.*, **367**, L33 (1996).
20. M. R. Vogt, A. Lachenwitzer, O. M. Magnussen, and R. J. Behm, *Surf. Sci.*, **399**, 49 (1998).
21. L.- J. Wan and K. Itaya, *J. Electroanal. Chem.*, **473**, 10 (1999).
22. B. J. Wiersma, Y. Tak, and K. R. Hebert, *J. Electrochem. Soc.*, **136**, 371 (1991).
23. C. G. Dunn and R. B. Bolon, *J. Electrochem. Soc.*, **116**, 1050 (1969).
24. N. Sinha, M.S. Thesis, Iowa State University, Ames, IA (1999).
25. J. Newman, *Electrochemical Systems*, 2nd ed., p. 43, Prentice-Hall, Englewood Cliffs, NJ (1991).

Downloaded on 2014-02-10 to IP 129.186.176.91 address. Redistribution subject to ECS license or copyright; see ecsdl.org/site/terms_use